10.1109/TIM.2021.3055829

High-linearity Front-end Circuit for Remote Grounded Capacitive Sensors

Marcelo A. Haberman, Enrique M. Spinelli,
and Ferran Reverter

***Abstract*—This paper presents a novel front-end circuit for remote grounded capacitive sensors. The circuit is insensitive to amplifier input capacitance and stray interconnecting-cable capacitances. It does not rely on neutralization or compensation techniques that require manual adjustments and high-accuracy reference components. The proposed solution reduces the circuit input capacitance below a few femptofarads using a simple but properly shielded custom transformer. In addition, the circuit keeps a non-linearity error below 0.01% when measuring capacitances of units or tens of picofarad, even with up to 12 m interconnecting cables.**

***Index Terms*—Active shielding, capacitive sensor, front-end circuit, grounded capacitive sensor, sensor interface electronics.**

I. Introduction

CAPACITIVE sensors are widely employed in laboratory and industrial applications to sense many physical and chemical quantities, such as: linear and angular displacement [1], relative humidity [2], liquid level [3], and microdroplet detection [4]. In comparison with other types of sensor, capacitive sensors result in low-power, low-cost, and robust sensing solutions. They also offer high sensitivity, high resolution, and broad bandwidth whenever they are read by a well-designed measurement circuit.

Capacitive sensors can be classified into two groups [2], [5], [6]: 1) floating capacitive sensors, where the two sensor electrodes are available to the measurement circuit, and 2) grounded capacitive sensors, where one of the two electrodes is connected to ground. The latter is also called single-electrode or one-terminal capacitive sensor. Sensor systems favor floating over grounded capacitive sensors, since the corresponding measurement circuit can be more easily designed. This is especially the case when the sensor is remote and, therefore, it is connected to the circuit through a shielded cable with significant parasitic capacitances that should not affect the measurement. However, some sensing applications force/imply the grounding of one of the electrodes and, then, the use of a grounded capacitive sensor is mandatory. This occurs, for example, in the following applications: linear/angular displacement sensors where the shaft is grounded [1], distance/proximity sensors where the target is grounded [5], [7], liquid-level sensors in metallic grounded storage tanks [8], [9], and non-contact line-voltage measurement [10].

Several measurement circuits have been proposed in the literature for grounded capacitive sensors. The simplest design solution is that based on a microcontroller measuring the discharging time of an RC circuit that includes the capacitive sensor [11]–[13]. This, however, does not have any mechanism to compensate for the effects of the parasitic capacitances of the interconnecting cable. Another approach is the use of a relaxation oscillator [9], [14]–[16], with an output period that depends on the sensor capacitance. In such oscillators, the active-shielding technique is generally applied to reduce the effects of cable parasitic capacitances. In [14], a non-linearity error (NLE) of 0.03% Full-Scale Span (FSS), 0.06%, and 0.12% are reported for an interconnecting cable of 1, 5, and 10 m, respectively. In [15], the previous performance is improved and the NLE equals 0.03% for a cable length of 30 m. Nevertheless, in both cases [14], [15], the sensor capacitance range is relatively high (to be precise, 330 pF) and a measurement of the offset capacitance (due to the devices and tracks of the printed circuit board, PCB) is required. Measurement circuits with a sinusoidal excitation (instead of square as occurs before) of the capacitive sensor have also been suggested [1], [7], [10], [17], with the advantage that an appropriate selection of the excitation frequency can make the sensor parasitic components negligible. A passive shielding of the interconnecting cable is applied in [7], whereas an active shielding in [1]. In both cases, however, a capacitor of the circuit must be adjusted to the value of the offset capacitance and, in addition, no data are provided about the performance of the circuit for different cable lengths. In [10], a system calibration measures the offset capacitance before the normal operation, where the offset capacitance is digitally subtracted.

There are also commercial high-performance integrated circuits (IC) specifically designed for the measurement of grounded capacitive sensors, such as the AD7747 and AD7147 from Analog Devices; the latter is employed, for instance, in [18]. Regrettably, the response of these ICs clearly deteriorates when the shield capacitance is higher than 150-200 pF, that corresponds to a cable length of about 1.5-2 m.

Taking into account the limitations indicated before, this paper proposes a novel front-end circuit for remote grounded

Manuscript received Month xx, 2xxx; revised Month xx, xxxx; accepted Month x, xxxx.

This work was supported in part by the CONICET under Project PIP-0558, in part by the UNLP under Projects I254 and PPID/I014, in part by the Agencia I+D+i under Project PICT-2015/2257, and in part by the Spanish Ministry of Economy and Competitiveness and the European Regional Development Fund under project TEC2016-76991-P.

Marcelo A. Haberman and Enrique M. Spinelli are with the Institute LEICI, UNLP, CONICET, La Plata 1900, Argentina (e-mail: marcelo.haberman@ing.unlp.edu.ar).

Ferran Reverter is with the Department of Electronic Engineering, Universitat Politècnica de Catalunya-BarcelonaTech, Castelldefels 08860 (Barcelona), Spain (e-mail: ferran.reverter@upc.edu)

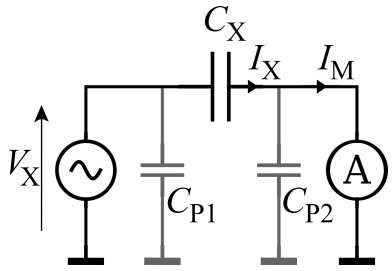

Fig. 1: AC bridge technique for measurement of a floating capacitance C_X.

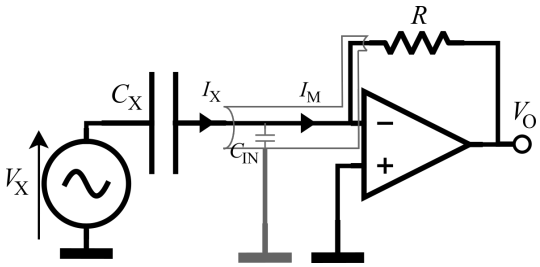

Fig. 2: Implementation of the AC bridge technique with a Trans-Impedance Amplifier as a current detector to measure a floating capacitance C_X.

capacitive sensors, using sinusoidal excitation and active-shielding techniques. The proposed circuit relies on the AC bridge with current-detection method shown in Fig. 1, which is the reference technique for floating capacitive sensors [19]. In this case, one electrode of the capacitive sensor is connected to a voltage source V_X and the other to the input of a current detector with very low input impedance, such as a transimpedance amplifier (TIA) [20] (Fig. 2) or a charge amplifier [21]. To adapt this technique, intended for floating capacitances, to grounded capacitive sensors, it is proposed to exchange the positions of the voltage source V_X and the capacitance C_X to be measured. The main challenge of this approach is the implementation of a floating voltage source V_X, which is implemented herein by means of a particularly shielded transformer. Using this technique, the proposed circuit offers a NLE smaller than 0.01% FSS when measuring capacitances in the range of 10 pF for a cable length of 12 m, which is a top performance in comparison with the state of the art. In addition, the proposed circuit does not require any measurement of the offset capacitance generated by the devices and tracks of the PCB since this is almost zero thanks to the smart shielding applied.

The paper is organized as follows. Section II describes the operating principle of the proposed circuit. Section III presents the design of the shielded transformer. Section IV analyses the effect of cable length on the measurements. Sections V and VI explain the materials and methods, and the corresponding experimental results, respectively. Finally, Section VII draws the main conclusions.

II. Operating Principle

The aforementioned technique of the AC bridge circuit, depicted in Figs. 1 and 2, measures the capacitance C_X of a floating sensor rejecting the effects of stray/parasitic capacitances C_{P1} and C_{P2} at its nodes. These correspond to leads and cable capacitances, but C_{P2} also includes the TIA input capacitance and the effects of PCB traces. In Fig. 2, C_{P1} is removed because it has no effect on circuit performance (note that it is in parallel with the input voltage source) and C_{P2} is renamed as C_{IN}, to be taken into account in a further error analysis. The ideally null input impedance of the TIA ensures $I_M = I_X$ independently of C_{IN} leading to:

$$I_M = I_X = j \cdot \omega_X \cdot C_X \cdot V_X, \tag{1}$$

where ω_X is the angular frequency of the sinusoidal voltage source V_X.

Then, the output voltage V_O, given by (2), is proportional to C_X without any offset due to parasitic capacitances, and the capacitance C_X can be computed by (3).

$$V_O = -I_M \cdot R = -j \cdot \omega_X \cdot C_X \cdot V_X \cdot R \tag{2}$$

$$C_X = \frac{|V_O|}{\omega_X \cdot V_X \cdot R} \tag{3}$$

If the impedance to measure is not purely capacitive, then C_X can be estimated as:

$$C_X = \frac{V_{OQ}}{\omega_X \cdot V_X \cdot R}, \tag{4}$$

where V_{OQ} is the component of V_O in quadrature with V_X.

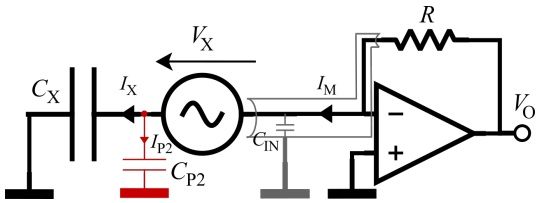

Fig. 3: Adaptation of the AC bridge for the measurement of a grounded capacitance C_X, by interchanging C_X and V_X in the original circuit shown in Fig. 2. It is shown the effect of parasitic capacitance to ground C_{P2} on the free terminal of C_X.

The proposed front-end circuit, depicted in Fig. 3, is an adaptation of the well-known AC bridge to measure grounded capacitances, where the positions of V_X and C_X are interchanged with respect to Fig. 2. A floating AC driving voltage V_X is used to deal with the grounded capacitance. It is connected in series with C_X, whereas the non-inverting input of the operational amplifier (OA) is grounded as in the original circuit of Fig. 2. There, C_{P1} is shunted by the grounded connection of C_X, while the negative feedback sets the OA inverting input to virtual ground and no current flows through the input capacitance C_{IN}. Therefore, if C_{P2} is negligible (as explained later in section II-A), $I_M = I_X$ and equations (1) to (4) are still valid (without the minus sign in (2)) and the proposed circuit is insensitive to C_{P1} and C_{IN} as the well-known AC bridge is.

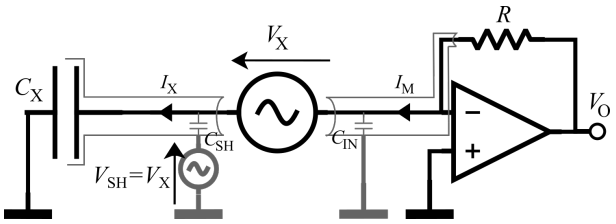

Fig. 4: The proposed circuit for the measurement of grounded capacitances with the corresponding guarding.

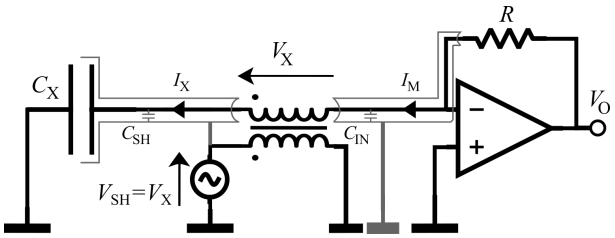

Fig. 5: Implementation of the solution proposed in Fig. 4 by means of a 1:1 voltage transformer.

A. Active shielding

The front-end circuit of Fig. 3 requires the use of guarding techniques to avoid picking up unwanted currents and capacitive couplings. There are two nodes to guard, one is the inverting input of the OA that is passively shielded at ground potential. The other node consists of the non-grounded terminal of C_X, the interconnection cable and the terminal of V_X that is not at the OA inverting input. If left unshielded, this node is capacitively coupled to ground through C_{P2} and drains a current I_{P2}, thus affecting the measurement. To avoid this, and remain the measurement insensitive to C_{P2}, this node must be actively-guarded to a voltage equal to V_X. This active shield, that is shown in Fig. 4, is driven by $V_{SH} = V_X$, and thus no current flows through the capacitance of the interconnection cable C_{SH}.

B. Implementation with a 1:1 transformer

The main challenge of the proposed circuit is the implementation of the floating voltage source V_X. Fig. 5 shows a solution by using a 1:1 voltage transformer (VT) to produce a floating V_X generator from a grounded one V_{SH}. This later is also used to drive the active guard.

Nevertheless, the parasitic capacitances of the winding of the VT jeopardize the proposed solution. As Fig. 6a shows, the parasitic coupling to ground, or even to a driven shield, affects the measurement by means of a current I_S drained from the secondary winding, i.e.: $I_M = I_X + I_S \neq I_X$. Therefore, the conventional active o passive shielding schemes are not applicable herein. Ideally, to null I_S, the secondary winding should be guarded by an active shield that tracks the voltage distributed along the length of the winding, as it is depicted in Fig. 6b.

The way proposed to meet the previous shielding requirement is by winding together the primary and secondary coils using a coaxial cable on a toroidal magnetic core, as shown in Fig. 7. The shield of the coaxial cable is the primary winding driven by V_{SH}, that actively and gradually shields (as represented in Fig. 6b) the secondary winding implemented by the central conductor of the coaxial cable.

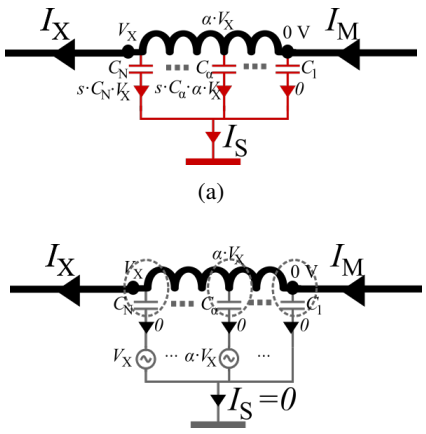

Fig. 6: (a)Effect of equipotential shield on parasitic currents of secondary winding. (b)Ideally gradual shielding of secondary winding.

III. Design of the transformer

The transformer, shown in block # 2 in Fig. 10, was built by winding 39 turns of coaxial cable RG174U [22] around a toroidal core CF195/T5818C from Cosmo Ferrites. Both ends of the coaxial cable were terminated with male BNC connectors.

The transformer was modelled by the equivalent circuit with lumped elements [23] of Fig. 8, where R_A and L_A are the resistance and the dispersion inductance of the primary winding (i.e. the shield of the coaxial cable), R_B and L_B are the resistance and the dispersion inductance of the secondary winding (i.e. the inner conductor of the coaxial cable), L_M is the magnetizing inductance, R_M represents the power looses of the magnetic core, and C_{VT} represents the distributed capacitance of the coaxial cable that is represented by two lumped capacitance of $0.5 \cdot C_{VT}$. These parameters were measured at $\omega_X = 2\pi 40$ kHz with a LCR meter GW-Instek LCR-819, and are shown in Table I.

The voltage ratio k, of the unloaded transformer, is defined

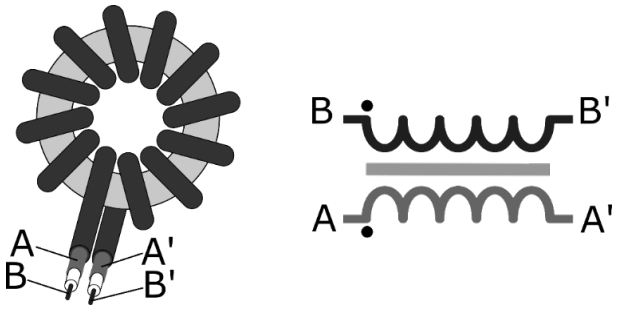

Fig. 7: Proposed transformer to achieve a gradual active shielding of the secondary winding.

TABLE I: Measured components of the transformer model.

parameter	measured value
C_{VT}	257 pF
L_M	9 mH
R_M	130 kΩ
R_A	0.1Ω
L_A	0.5μH
R_B	0.5Ω
L_B	0.5μH

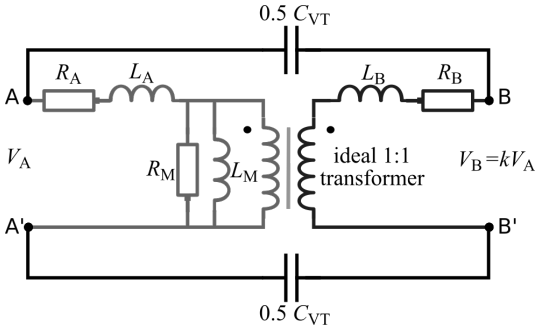

Fig. 8: Circuital model of implemented transformer.

by (5):

$$k = \frac{V_B}{V_A} = \frac{(j\omega_X L_M)\,||R_M}{(j\omega_X L_M)\,||R_M + j\omega_X L_A + R_A}. \quad (5)$$

This equation is also valid when the secondary winding is loaded by the capacitance C_X (as in Fig. 5), given that it represents a negligible load effect to the transformer at the working frequency ω_X. Computing (5) for the measured components listed in Table I, we have $k = 0.999943 + j \cdot 00004 \approx 1$, which implies that the implemented VT behaves like an ideal 1:1 transformer.

In the circuit shown in Fig. 5, C_X is in series with the secondary of the transformer that offers an impedance Z_B. At the operating frequency of the circuit, the magnetizing impedance is much higher than that due to R_A-L_A. In such conditions and assuming $k = 1$, the impedance of the transformer referred to the secondary side can be approximated to $Z_B = R_A + R_B + j\cdot\omega_X\cdot(L_A + L_B)$. This impedance, however, can be neglected given that $\left|(j \cdot \omega_X \cdot C_X)^{-1}\right| >> |Z_B|$.

The experimental characterization of the designed VT also showed that its core has a saturation volt-per-hertz ratio of, at least, 10 V/kHz. This ratio is more than a hundred times higher than those applied in the experimental setup and, hence, saturation effects will be completely negligible during the tests.

IV. Analysis of the effects of cable length

To explain the effects of the interconnecting cable on the measurement of C_X, a more complete circuital model is required (see Fig. 9). It considers the finite OA open-loop gain $A(s)$ and the following parasitic capacitances: C_{IN} introduced by the input of OA and the shielding of input node, C_{VT} introduced by the transformer, and C_{SH} which is the capacitance of the interconnecting cable between the sensor and the front-end with a typical relationship of 100 pF/m. The

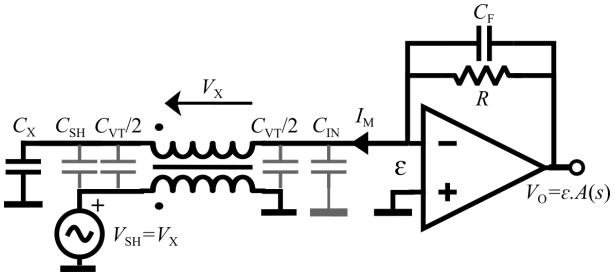

Fig. 9: Extended model to explain the effect of using long interconnecting cables in remote measurements.

feedback capacitance C_F (in the order of picofarads) is added to compensate for the TIA frequency response. The parasitic capacitance between the input and the output of the OA (due to the package of both the OA and R, and the traces of the PCB) is not considered here, since it is at most tenths of picofarad, which represents less than 10% of C_F. For the sake of clarity, the inductance and resistance introduced by the transformer are neglected and also the interconnecting cable inductance, given that these components introduce high order singularities on the frequency response that does not affect the output at ω_X.

Considering the circuit of Fig. 9, assuming an integrating transfer function for the OA [24] given by:

$$A(s) = \frac{\omega_{GBP}}{s}, \quad (6)$$

where ω_{GBP} is the Gain-Bandwidth product, and following the steps indicated in the Appendix, we can find the following transfer function of the front-end circuit:

$$T(s) = \frac{V_O(s)}{V_X(s)} = s \cdot C_X \cdot R \left[\frac{1}{1 + s(2\zeta/\omega_n) + s^2/\omega_n^2}\right] = s \cdot C_X \cdot R \cdot T_2(s), \quad (7)$$

which is similar to (2), but affected by an underdamped second order low-pass response $T_2(s)$ with a natural frequency $\omega_n = \sqrt{\frac{\omega_{GBP}}{R(C_X + C_{IN} + C_{VT} + C_{SH})}}$ and a damping factor $\zeta = \omega_n \cdot R \cdot C_F/2$.

For low enough frequencies ($\omega_X << \omega_n$), the measurement is independent of the parasitic capacitances C_{IN}, C_{VT} and C_{SH}, and (7) reduces to (2). However, for long cables, the value of ω_n is reduced, producing a factor $T_2(s)$ whose magnitude becomes greater than unity, thus resulting in a gain error.

V. Materials & methods

A. Experimental setup

Several tests were done to assess the proposed technique, through the experimental setup shown in Fig. 10. A set of discrete ceramic capacitors (leaded/through hole) in two ranges 0-10 pF and 10-100 pF were measured with the proposed technique (Fig. 11) and by using the standard AC bridge method (Fig. 12), which was used as a "gold standard". Both measurements were made using a 4 1/2-digit lock-in amplifier (Stanford Research SR830), shown as the block #6 in Fig. 10, which injects the reference voltage V_X at a frequency of

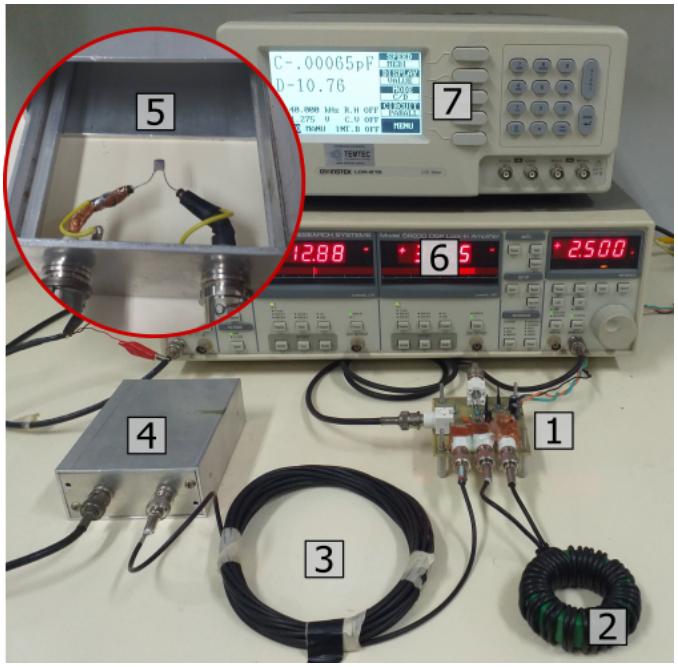

Fig. 10: Photograph of the experimental setup and its main components, arranged to measure grounded capacitors with the 6 m cable. (1): PCB with the analog front-end - (2): voltage transformer - (3): interconnecting cable - (4): shield box - (5): detail of a ceramic capacitor mounted inside the shield box - (6): lock-in amplifier - (7): LCR meter.

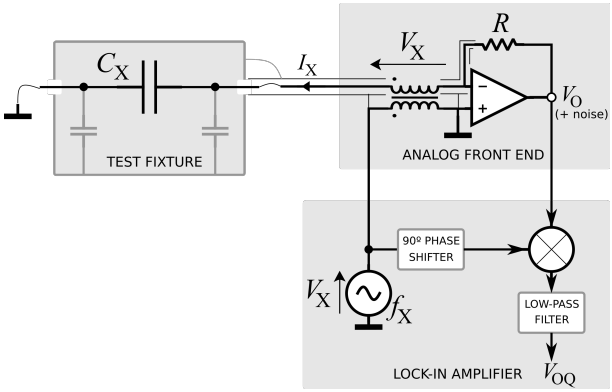

Fig. 11: Experimental setup to assess the proposed solution for the measurement of grounded capacitances.

40 kHz and measures the quadrature component V_{OQ}. The amplitude of V_X was set according to the capacitance range: 2.5 V_{RMS} for 0-10 pF, and 250 mV_{RMS} for 10-100 pF.

In order to avoid variations on measured capacitances due to parasitic coupling to the environment, an aluminium shield box was used as a test fixture to preserve the capacitors under test (#4 and #5 in Fig. 10). The capacitances were measured by the two methods without removing nor moving them from the shield box.

The front-end circuit was built in a PCB (#1 in Fig. 10) that contains the TIA with its shields and BNC connectors for V_X, V_O, to connect the 1:1 transformer, and for the cable that links it with the shield box. The TIA is based on the OPA320

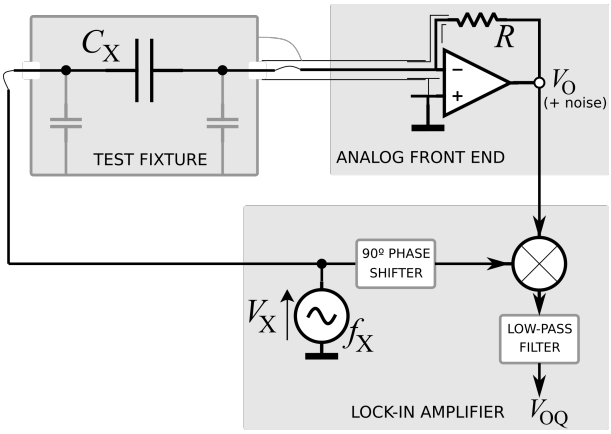

Fig. 12: Experimental setup to measure with the floating reference technique.

from Texas Instruments in a SOT-23 package, supplied at ±2.5 V, with a feedback resistor $R = 100$ kΩ in parallel with a capacitor $C_F = 2.2$ pF. The same circuit allows us to switch between the proposed measurement technique (Fig. 11) and the standard method for floating capacitances (Fig. 12).

The capacitors used in the test were also measured by a general purpose LCR meter GW-Instek LCR-819 (#7 in Fig. 10). Given the limited accuracy of this instrument, these data were used just to compute the proportionality constant K that relates the measured voltage V_{OQ} with the capacitance: $C_X = K \cdot V_{OQ}$. For both ranges of capacitance under test, we calculated the corresponding K value by means of a linear regression (minimizing the mean squared error) between LCR measurements and V_{OQ} for the floating reference case (second and fourth columns of Tables II and III).

B. Non-Linearity Error (NLE) analysis

The assessment of NLE of the proposed technique was performed separately for each capacitance range. Each capacitor was placed in the shield box and three measurements were performed: one with the LCR meter and the other two using the lock-in amplifier, with the proposed front-end (Fig. 11) and with the floating reference technique (Fig. 12). All these measurements were made with a 1 m RG174U-type coaxial cable interconnecting the PCB with the shield box.

Using the K value indicated before (obtained from the reference floating case) and the output voltages from the setups in Figs. 11 and 12 (third and fourth columns in Tables II and III), we estimated the value of the capacitance in grounded and floating modes, identified as C_X^G and C_X^F, respectively. Then, C_X^G was represented versus C_X^F and a straight line was fitted by means of the least-squares method to calculate the NLE. This was then expressed as a percentage of the FSS.

C. Errors induced by cable length

The capability of the technique proposed in Fig. 11 to measure remote grounded capacitances was tested by modifying the length of the coaxial cable that links the front-end with the capacitance C_X. Three RG174U-type coaxial cables of 1 m,

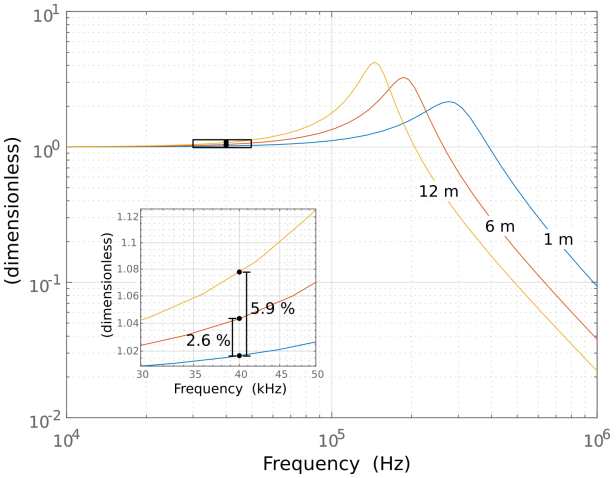

Fig. 13: Simulated frequency response of $|T_2(s)|$ for three different length cables, and its effects at ω_X.

6 m and 12 m in length, were used to measure four capacitors chosen on the 0-10 pF range. For each of the four capacitors, the resulting V_{OQ} was measured for every interconnecting cable without removing the capacitor from the shield box between measurements.

As was aforementioned, increasing the cable length results in a systematic gain error. To predict the changes on gain with the increase of C_{SH}, $|T_2(s)|$ was computed for C_{SH}: 100, 600 and 1200 pF, corresponding to cables of 1, 6 and 12 m respectively. For the remaining circuit parameters, the following values were considered: C_X=10 pF, R=100 kΩ, C_F=2.2 pF, $\omega_{GBP} = 2\pi 20$ MHz, C_{IN} = 9 pF, and C_{VT}=257 pF. The computed $|T_2(s)|$ curves, for each value of C_{SH}, are plotted in Fig. 13. At the operating frequency of 40 kHz, it can be seen the increase in the output voltage of 2.6% and 5.9% for 6 and 12 m cables, relative to the 1-meter cable case.

VI. Experimental Results and Discussion

A. Non-Linearity Error analysis

The measurements performed for each test capacitor are resumed in tables II and III, for the 0-10 pF and 10-100 pF ranges, respectively. For each range, the constant K was computed, being K=16.10 [pF/V] and K=158.8 [pF/V], respectively.

Figs. 14 and 15 show the NLE analysis of the grounded measurements executed with the proposed method, relative to the floating measurement. For the 0-10 pF range, the maximum NLE is 0.01% FSS, and 0.006% FSS for the 10-100 pF range. Both ranges show a very low residual offset capacitance, to be precise: -0.8 fF and -11.6 fF in Figs. 14 and 15, respectively. This offset corresponds to an error of 0.01% FSS.

B. Errors induced by cable length

The experimental results for different cable lengths in the setup shown in Fig. 11 are resumed in Table IV. Accordingly, the higher the length, the higher the value of V_{OQ}, as predicted in Fig. 13. Using the K value estimated before for such a range, the value of C_X^G was estimated and represented in Fig.

TABLE II: Experimental results for 0-10 pF range.

Nominal value [pF]	LCR meter [pF]	V_{OQ} [mV] (grounded)	V_{OQ} [mV] (floating)
0 (empty box)	—	0.013	0.053
1.2	1.372	85.24	85.23
1.8	1.936	120.27	120.25
2.2	2.300	142.85	142.83
3.3	3.475	215.8	215.8
4.7	4.810	298.8	298.7
5.6	6.158	382.6	382.4
6.8	7.101	441.1	441.0
8.2	8.539	530.6	530.4
10.0	10.550	655.6	655.3

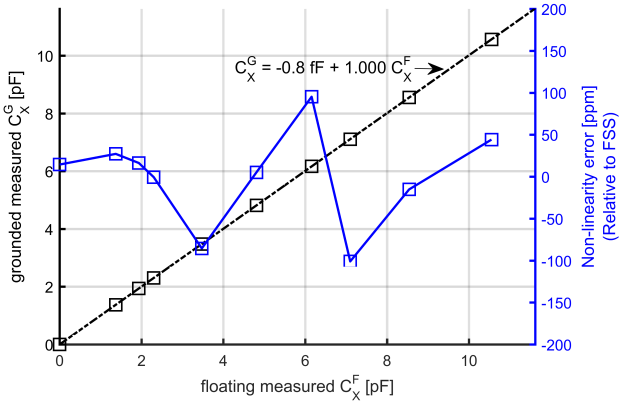

Fig. 14: Linearity analysis for measurements in the 0-10 pF range.

TABLE III: Experimental results for 10-100 pF range.

Nominal value [pF]	LCR meter [pF]	V_{OQ} [mV] (grounded)	V_{OQ} [mV] (floating)
10	10.472	65.77	65.80
18	18.942	119.05	119.04
33	33.372	209.9	209.8
68	69.110	435.3	435.0
82	83.900	528.9	528.6
100	96.850	610.7	610.3

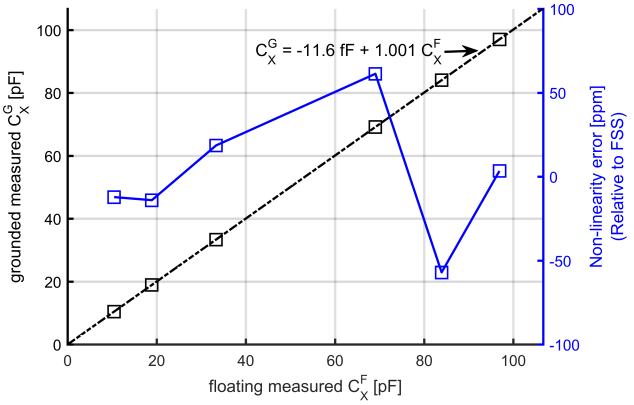

Fig. 15: Linearity analysis for measurements in the 10-100 pF range.

TABLE IV: Experimental results for different cable lengths.

Nominal value [pF]	V_{OQ} [mV] (1m cable)	V_{OQ} [mV] (6m cable)	V_{OQ} [mV] (12m cable)
1.2	85.94	88.03(+2.4%)	90.97(+5.8%)
2.2	144.04	147.50(+2.4%)	152.34(+5.8%)
4.7	299.9	307.1(+2.4%)	317.0(+5.7%)
10.0	657.2	672.9(+2.4%)	694.7(+5.7%)

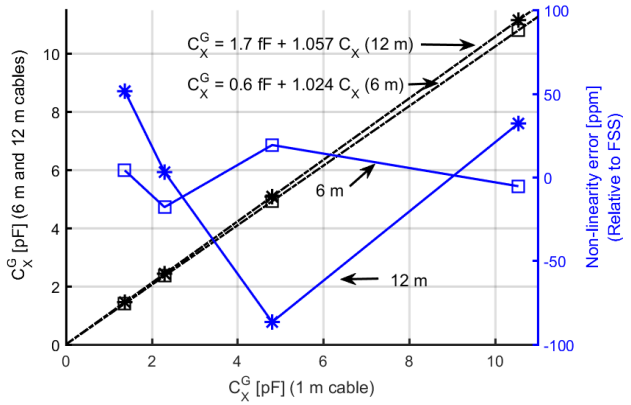

Fig. 16: Linearity analysis for measurements in the 0-10 pF range for two different cable lengths.

16 versus that obtained for the 1 m case. It can be seen that the linearity is preserved with long cables, but, the longer the cable, the greater the gain error. These experimental deviations are very close to the expected theoretical errors of 2.6% and 5.9% predicted in section V-C.

C. Discussion

A comparison of the performance of the proposed front-end circuit vis-à-vis the existing circuits for grounded capacitive sensors is summarized in Table V. The proposed circuit employs a sinusoidal excitation, as in [1], [7], [10], but it relies on a transformer that acts as a floating voltage source. The active shielding technique is applied herein to the interconnecting cable, as in [1], [10], [14], [15], but in addition the transformer is subjected to a gradual active shielding. Thanks to the application of these techniques, the proposed circuit offers the following advantages: 1) capability to measure capacitances in a low-value range (to be precise, 0-10 pF range), 2) an extremely low value of the circuit offset capacitance (e.g. -0.8 fF in the 0-10 pF range) and, hence, there is no need to apply any offset compensation, and 3) a very small non-linearity error (0.01%) even when a 12-m interconnecting cable is employed. In terms of the previous three points, the proposed circuit clearly outperforms the circuits suggested so far in the literature.

VII. Conclusions

A novel front-end circuit for remote grounded capacitive sensors, which reaches the performance of those for the floating counterparts, has been presented. The circuit outperforms the current state of the art front-ends for this type of sensors, with a NLE smaller than 0.01% and a negligible offset capacitance (a few femtofarads) when measuring capacitances in the 0-10 pF range with a cable length up to 12 m. The very small offset capacitance introduced by the presented circuit makes the measurement and compensation of input parasitic capacitance unnecessary. This enables the measurement of remote grounded capacitances without any manual adjustment.

In some applications as capacitive liquid level sensors [14], the sensor itself has an inherent offset capacitance, that is imposed by the sensor geometry and, therefore, is part of C_X. In these kinds of applications, an offset calibration/compensation is still necessary, but the presented front-end could contribute to make that calibration more stable, being insensitive to changes or drifts on C_{IN}.

Appendix

To obtain the transfer function of (7) from the circuit of Fig. 9, the secondary winding was replaced by an independent generator V_X and the OA open-loop gain was modelled as another independent generator $\epsilon = \frac{V_O}{A(s)}$ connected to the noninverting input of an ideal OA (see Fig. 17). Therefore, applying superposition of voltages sources it can be obtained the following partial expressions:

$$V_O|_{V_X}(s) = V_X(s) \cdot s \cdot (C_X + C_{SH} + 0.5C_{VT}) \cdot Z_F \quad \text{(A.1)}$$

$$V_O|_{V_{SH}}(s) = -V_{SH}(s) \cdot s \cdot (C_{SH} + 0.5C_{VT}) \cdot Z_F \quad \text{(A.2)}$$

$$V_O|_{\epsilon}(s) = -\epsilon\,[1 + s \cdot (C_X + C_{SH} + C_{VT} + C_{IN}) \cdot Z_F] \quad \text{(A.3)}$$

where $Z_F = R/(1 + s \cdot C_F \cdot R)$.

Combining (A.1), (A.2) and (A.3), replacing for $\epsilon = V_O/A(s)$ and $V_{SH} = V_X$, and solving for V_O results:

$$V_O(s) = V_X(s)\frac{s \cdot C_X \cdot Z_F}{1 + \frac{1}{A(s)} + \frac{s \cdot C_{EQ} \cdot Z_F}{A(s)}}, \quad \text{(A.4)}$$

where $C_{EQ} = C_X + C_{SH} + C_{VT} + C_{IN}$.

Considering that $1 + \frac{1}{A(s)} \approx 1$, and replacing for $A(s) = \omega_{GBP}/s$ and $Z_F = R/(1 + s \cdot C_F \cdot R)$, expression (A.5) is obtained, that corresponds to (7).

$$V_O(s) = V_X(s)\frac{s \cdot C_X \cdot R}{1 + s \cdot R \cdot C_F + \frac{s^2 \cdot C_{EQ} \cdot R}{\omega_{GBP}}} \quad \text{(A.5)}$$

References

[1] N. Anandan and B. George, "A wide-range capacitive sensor for linear and angular displacement measurement," *IEEE Trans. Ind. Electron.*, vol. 64, no. 7, pp. 5728–5737, 2017.

[2] A. U. Khan, T. Islam, B. George, and M. Rehman, "An efficient interface circuit for lossy capacitive sensors," *IEEE Trans. Instrum. Meas.*, vol. 68, no. 3, pp. 829–836, 2018.

[3] K. Loizou and E. Koutroulis, "Water level sensing: State of the art review and performance evaluation of a low-cost measurement system," *Measurement*, vol. 89, pp. 204–214, 2016.

TABLE V: Comparison study

	[13]	[14]	[15]	[7]	[1]	[10]	**This work**
Operating principle	RC charge-discharge	CT-RO	CT-RO	AC bridge	AC bridge	AC bridge	**Trafo-based AC bridge**
Excitation wave	Square	Square	Square	Sine	Sine	Sine	**Sine**
Measurement range (pF)	[100, 225]	[27, 330]	[10, 330]	[150, 1100]	[50, 110]	[1, 5]	**a) [0, 10] b) [10, 100]**
Circuit offset capacitance	17.4 pF	NR	NR	NR	NR	1.5 pF	**a) -0.8 fF b) -11.6 fF**
Offset compensation	SW-C with stored value	3-signal auto-calibration	3-signal auto-calibration	MA of a capacitor	MA & SW-C	SW-C	**Not required**
Max. cable length (MCL) (m)	NS	10	30	10 $^{(a)}$	<1	1.5	**12**
Max. NLE (%) at MCL	NS	0.12	0.03	0.025	0.7 $^{(b)}$	0.2	**0.01**
Shielding type	NS	Active - Feedforward	Active - Feedforward	Passive	Active	Active	**Active and gradual**

Abbreviations: CT-RO: Charge-transfer based relaxation oscillator, SW-C: Software correction/calibration, MA: Manual adjustment, NS: Not studied, NR: Not reported.
Notes: $^{(a)}$ Emulated by a capacitance, not a real cable. $^{(b)}$ It corresponds to the sensor together with the circuit.

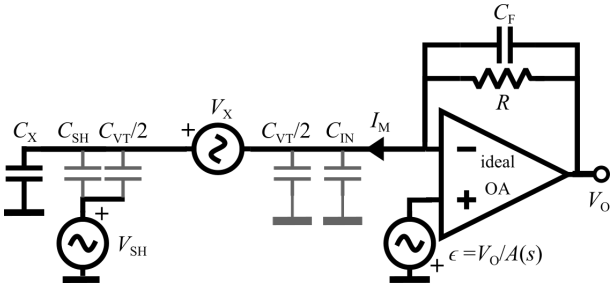

Fig. 17: Extended model to explain the effect of using long interconnecting cables in remote measurements.

[4] Z. H. Zargar and T. Islam, "A novel cross-capacitive sensor for noncontact microdroplet detection," *IEEE Trans. Ind. Electron.*, vol. 66, no. 6, pp. 4759–4766, 2018.

[5] W. C. Haase, "Digital measurement circuit and system using a grounded capacitive sensor," U.S. Patent 6 700 392, Mar. 2, 2004.

[6] Y. Jung, Q. Duan, and J. Roh, "A 17.4-b delta-sigma capacitance-to-digital converter for one-terminal capacitive sensors," *IEEE Trans. Circuits Syst. II*, vol. 64, no. 10, pp. 1122–1126, 2015.

[7] C. Baby and B. George, "A simple analog front-end circuit for grounded capacitive sensors with offset capacitance," in *2013 IEEE International Instrumentation and Measurement Technology Conference (I2MTC)*, pp. 1372–1375. IEEE, 2013.

[8] S. C. Bera, J. K. Ray, and S. Chattopadhyay, "A low-cost noncontact capacitance-type level transducer for a conducting liquid," *IEEE Trans. Instrum. Meas.*, vol. 55, no. 3, pp. 778–786, 2006.

[9] F. Reverter, X. Li, and G. C. Meijer, "Liquid-level measurement system based on a remote grounded capacitive sensor," *Sens. Actuators, A*, vol. 138, no. 1, pp. 1–8, 2007.

[10] M. A. Haberman and E. M. Spinelli, "A noncontact voltage measurement system for power-line voltage waveforms," *IEEE Trans. Instrum. Meas.*, vol. 69, no. 6, pp. 2790–2797, 2019.

[11] K. Chetpattananondh, T. Tapoanoi, P. Phukpattaranont, and N. Jindapetch, "A self-calibration water level measurement using an interdigital capacitive sensor," *Sens. Actuators, A*, vol. 209, pp. 175–182, 2014.

[12] B. Jin, Z. Zhang, and H. Zhang, "Structure design and performance analysis of a coaxial cylindrical capacitive sensor for liquid-level measurement," *Sens. Actuators, A*, vol. 223, pp. 84–90, 2015.

[13] Z. Czaja, "A measurement method for capacitive sensors based on a versatile direct sensor-to-microcontroller interface circuit," *Measurement*, vol. 155, p. 107547, 2020.

[14] F. Reverter, X. Li, and G. C. Meijer, "A novel interface circuit for grounded capacitive sensors with feedforward-based active shielding," *Meas. Sci. Technol.*, vol. 19, no. 2, p. 025202, 2008.

[15] A. Heidary and G. C. Meijer, "An integrated interface circuit with a capacitance-to-voltage converter as front-end for grounded capacitive sensors," *Meas. Sci. Technol.*, vol. 20, no. 1, p. 015202, 2009.

[16] A. Ahmadpour Bijargah, A. Heidary, P. Torkzadeh, and S. Nihtianov, "An accurate and power-efficient period-modulator-based interface for grounded capacitive sensors," *Int. J. Circuit Theory Appl.*, vol. 47, no. 8, pp. 1211–1224, 2019.

[17] R. Joarder and C. S. Anoop, "A linear front-end circuit for offset-affected grounded capacitive sensors," in *TENCON 2019-2019 IEEE Region 10 Conference (TENCON)*, pp. 2280–2284. IEEE, 2019.

[18] S. Qiu, Y. Huang, X. He, Z. Sun, P. Liu, and C. Liu, "A dual-mode proximity sensor with integrated capacitive and temperature sensing units," *Meas. Sci. Technol.*, vol. 26, no. 10, p. 105101, 2015.

[19] S. M. Huang, A. L. Stott, R. G. Green, and M. S. Beck, "Electronic transducers for industrial measurement of low value capacitances," *J. Phys. E: Sci. Instrum.*, vol. 21, no. 3, p. 242, 1988.

[20] F. Aezinia and B. Bahreyni, "An interface circuit with wide dynamic range for differential capacitive sensing applications," *IEEE Trans. Circuits Syst. II*, vol. 60, no. 11, pp. 766–770, 2013.

[21] L. Areekath, B. George, and F. Reverter, "A closed-loop capacitance to pulse-width converter for single element capacitive sensors," in *2019 13th International Conference on Sensing Technology (ICST)*, pp. 1–5. IEEE, 2019.

[22] *Cable coaxial RG 174 U - Technical datasheet*, Indecable S.A., 2017, available at http://www.indeca.com.ar/files/36.pdf.

[23] R. S. Navarro, *Máquinas eléctricas*. McGraw-Hill, 1989.

[24] R. Pallás-Areny and J. G. Webster, *Analog signal processing*. John Wiley & Sons, 1999.